A Hybrid Cross-Connected Modular Multilevel Converter for Medium-Voltage Variable-Speed Motor Drives

Tan Luong Van[1,*]

ARTICLE INFO

Article history:
Received: 26 December 2022
Revised: 05 February 2023
Accepted: 14 February 2023

Keywords:
Capacitor voltage ripple
Common-mode voltage
Medium-voltage motor drives
Modular multilevel converters

ABSTRACT

This paper proposes a hybrid cross-connected modular multilevel converter (HC-MMC) for medium-voltage motor drive applications, which is able to reduce the submodule capacitor voltage ripple at the low-speed operation. Series-connection branches of capacitors and half-bridge submodules (HBSMs) are employed between the middle taps of the upper and lower arms in order to balance the power difference between both arms. With the proposed series-connection branch, the HC-MMC can be implemented with lower voltage rating of flying-capacitor compared to that in the flying-capacitor MMC topology. At the low-speed operation, the power difference between upper and lower arms is distributed through the series-connection branch, which leads to the reduction of submodule capacitor voltage ripple without the injection of the common-mode voltage in the motor side; as a result, there are no premature failure of winding insulation and motor bearing. Features and validity of the proposed HC-MMC and control scheme have been verified through simulation results.

1. INTRODUCTION

In the past decade, modular multilevel converter (MMC) has been regarded as one of the promising topologies for the medium/high-voltage applications due to its merits of low output voltage harmonics, modularity, scalability, and ability of fault-tolerant operation [1]–[5]. They have been used in high-voltage direct-current (HVDC) transmission systems [6, 7], static synchronous compensators (STATCOMs) [8], motor drives [9]–[14]. Nevertheless, in motor drive applications, one of the main challenges of the MMC is that the submodule (SM) capacitor voltage ripples are proportional to the amplitude of output current and inversely proportional to the fundamental frequency value [9]–[14]. As a result, the SM capacitor voltage ripples become larger under lower fundamental frequency operation, such as start-up and low-speed operation, which causes performance deterioration of MMC.

To mitigate the SM capacitor voltage ripple at low-speed operation, several studies have been performed [10], [12]–[14]. At a low-speed operation, the magnitude of capacitor voltage ripple can be reduced by the injection of high-frequency common-mode voltage (CMV) and circulating current in each leg, which supports to balance the power difference between upper and lower arms. Therefore, this control strategy is able to alleviate the SM capacitor voltage ripple, but the CMV issue exists in the motor side. It leads to the premature failure of winding insulation and motor bearing.

Other effective control schemes have been introduced to mitigate the voltage ripple on SM capacitor [15]–[19]. In [15]–[17], based on the operating speed regions, the average value of SM capacitor voltage is controllable instead of at the rated value, which results in the higher voltage ripple on SM capacitor with the lower average SM capacitor voltage. However, it is also necessary to inject the high-frequency CMV at the low-speed operation to alleviate the voltage ripple on SM capacitor. In [18, 19], instead of fully suppression of voltage, the SM capacitor voltage ripple is allowed to be fluctuated with a peak value lower than the maximum value of SM capacitor. Therefore, the amplitudes of voltage and current injections can be reduced.

Apart from improving control scheme, modified MMC topologies with auxiliary circuit have been presented to mitigate the SM capacitor voltage ripple without injecting the high-frequency CMV. In [20, 21], a flying-capacitor MMC has been presented to mitigate the SM capacitor voltage ripple without injecting the CMV. At the low-speed operation, the power difference between the upper and lower arms are balanced through the flying-capacitor branch. However, the voltage rating of the flying-capacitor is a half of DC-link voltage, which limits the overall voltage rating of the topology. In order to overcome this issue, the flying-capacitor has been substituted by a cross-connected branch which has the same number of half-bridge submodules (HBSMs) as one arm [22]. However, the system cost is

[1]*Department of Electrical and Electronics Engineering, Ho Chi Minh city University of Food Industry, Ho Chi Minh city, 760310, Vietnam.*
Corresponding author: Tan Luong Van; Phone: +84-909-653-157; Email: luongvt@hufi.edu.vn.

increased and the reliability is reduced since more active components are employed.

In this paper, a hybrid cross-connected MMC (HC-MMC) is proposed, where a series-connection branch consisting of HBSMs and flying-capacitor is suggested to redistribute the power difference between the upper and lower arm. The proposed topology has advantages of lower voltage rating of the flying-capacitor compared with the flying-capacitor MMC. In addition, it also requires lesser number of HBSMs compared with the topology with the cross-connected branch that has the same number of HBSMs as in one arm [22]. The feasibility of the proposed HC-MMC and control scheme have been validated through simulation results.

2. ANALYSIS OF SM CAPACITOR VOLTAGE RIPPLE IN THE TRADITIONAL MMC AT LOW-SPEED OPERATION

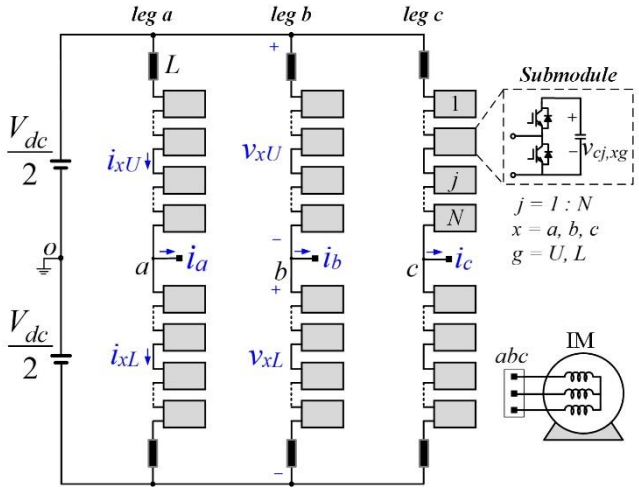

Fig. 1. Circuit configuration of the conventional MMC.

Fig. 1 shows the circuit configuration of the conventional MMC with the HBSM in the motor drive application. It includes three legs (x: a, b, c), each of which is comprised of an upper arm and a lower arm; each arm consists of N identical HBSMs. The AC output voltage and current are expressed as:

$$v_x = V_o \cos(\omega t + \delta_x), \tag{1}$$

$$i_x = I_o \cos(\omega t + \delta_x - \phi), \tag{2}$$

where, V_o and I_o are the voltage and current magnitudes, ω is the fundamental angular frequency, δ_x is the initial phase angle, and ϕ is the phase angle between voltage and current. The arm voltages and arm currents are expressed as:

$$v_{xU} = 0.5V_{dc} - V_o \cos(\omega t + \delta_x), \tag{3}$$

$$v_{xL} = 0.5V_{dc} + V_o \cos(\omega t + \delta_x), \tag{4}$$

$$i_{xU} = i_{circ,x} + 0.5 i_x, \tag{5}$$

$$i_{xL} = i_{circ,x} - 0.5 i_x, \tag{6}$$

where, v_{xU} and v_{xL} represent the upper and lower arm voltage, i_{xU} and i_{xL} are the upper and lower arm current, V_{dc} is the DC link voltage, and $i_{circ,x}$ is the circulating current within legs. According to the power balance between the DC-input and AC-output sides of the MMC, $i_{circ,x}$ is given as:

$$i_{circ,x} = \frac{v_x i_x}{V_{dc}}. \tag{7}$$

From (3), (5) and (7), the instantaneous power in the upper arm, p_{xU}, is:

$$\begin{aligned} p_{xU} &= v_{xU} i_{xU} \\ &= \frac{V_{dc} I_o}{4}\left(\cos(\omega t + \delta_x) - \frac{2V_o^2}{V_{dc}^2}\cos\phi\cos(\omega t + \delta_x - \phi) \right. \\ &\quad \left. - \frac{V_o}{V_{dc}}\cos(2\omega t + \delta_x - \phi) \right). \end{aligned} \tag{8}$$

The energy is obtained by integrating p_{xU} as

$$\begin{aligned} E_{xU} &= \frac{V_{dc} I_o}{4}\left(\frac{\sin(\omega t + \delta_x)}{\omega} - \frac{2V_o}{\omega V_{dc}^2}\cos\phi\sin(\omega t + \delta_x - \phi) \right. \\ &\quad \left. - \frac{V_o}{2\omega V_{dc}}\sin(2\omega t + \delta_x - \phi) \right). \end{aligned} \tag{9}$$

At the low-speed operation, the second and third terms can be neglected because ω becomes low. Therefore, (9) is derived as:

$$E_{xU} = \frac{V_{dc} I_o}{4}\frac{\sin(\omega t + \delta_x)}{\omega}. \tag{10}$$

From the upper arm energy, the peak-to-peak energy variation is achieved as:

$$\begin{aligned} \Delta E_{xg} &= E_{xg\_\max} - E_{xg\_\min} \\ &= \frac{V_{dc} I_o}{2\omega}. \end{aligned} \tag{11}$$

In addition, the relationship between the energy variation and N capacitor of SMs in the upper arm is:

$$\begin{aligned} \Delta E_{xU} &= N\left(\frac{1}{2} C v_{c\_\max}^2 - \frac{1}{2} C v_{c\_\min}^2 \right), \\ &= NC v_c \Delta v_{c\_pp} \end{aligned} \tag{12}$$

where, v_c is SM capacitor voltage and Δv_{c_pp} is the peak-to-peak SM capacitor voltage. From (11) and (12), Δv_{c_pp} is obtained as:

$$\Delta v_{c\_pp} = \frac{I_o}{2C\omega}. \tag{13}$$

It can be seen that the SM capacitor voltage ripple

becomes larger as speed decreases. If not suppressed, the performance of MMC-based motor drive system is significantly deteriorated.

3. PROPOSED HYBRID CROSS-CONNECTED MODULAR MULTILEVEL CONVERTER

3.1. Topology structure

Fig. 2 shows the circuit configuration of the modified flying-capacitor MMC. It is different from the conventional MMC that one inductor is added in each half-arm and the series-connection branch is used to link the middle taps of the upper and lower arms in each leg; the series-connection branch consists of 0.5*N* HBSMs. The HBSMs used in the series-connection branch has same voltage rating for IGBTs and capacitors as HBSMs in arms [22]. Hence, the modularity is maintained for the proposed topology. The capacitance of the flying-capacitor C_F is given as:

$$C_F = \frac{1}{(2\pi f_h)^2 L}, \tag{14}$$

where, f_h is the high-frequency and L is the half-arm inductor [20]. In addition, the voltage rating of the flying-capacitor is $V_{dc}/4$.

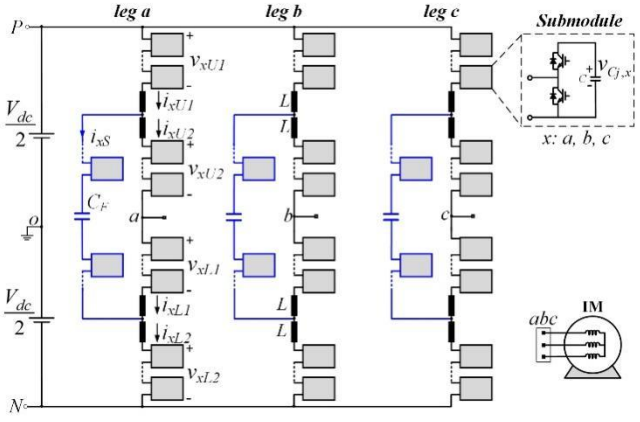

Fig. 2. Circuit configuration of the proposed hybrid cross-connected MMC.

3.2. Operating principle

In order to mitigate the large power fluctuation under low-speed operation, which causes the large SM capacitor voltage ripple [10], the series-connection branch is employed to redistribute the power imbalance between the upper and lower arms. The four half-arm voltages (v_{xU1}, v_{xU2}, v_{xL1} and v_{xL2}) are controlled as voltage sources and expressed as

$$v_{xU1} = 0.25V_{dc} - 0.5v_x - v_h, \tag{15}$$

$$v_{xU2} = 0.25V_{dc} - 0.5v_x + v_h, \tag{16}$$

$$v_{xL1} = 0.25V_{dc} + 0.5v_x - v_h, \tag{17}$$

$$v_{xL2} = 0.25V_{dc} + 0.5v_x + v_h, \tag{18}$$

where, v_h is the high-frequency component. v_h is expressed as:

$$v_h = V_h \sin(\omega_h t), \tag{19}$$

$$V_h = 0.25V_{dc}(1-m), \tag{20}$$

where, V_h is the amplitude of the high-frequency component and m is the modulation index.

The currents conducted in four half-arms (top and bottom half-arms in the upper and lower arms) and series-connection branches are i_{xU1}, i_{xU2}, i_{xL1}, i_{xL2} and i_{xS}. Those half-arm currents are expressed as:

$$i_{xU1} = i_{xd} + 0.5i_x + i_{xh}, \tag{21}$$

$$i_{xU2} = i_{xd} + 0.5i_x - i_{xh}, \tag{22}$$

$$i_{xL1} = i_{xd} - 0.5i_x - i_{xh}, \tag{23}$$

$$i_{xU2} = i_{xd} - 0.5i_x + i_{xh}, \tag{24}$$

where, i_{xd} and i_{xh} are the DC and AC-circulating currents, respectively.

From (15) and (21), the instantaneous power in the top half-arm of the upper arm, p_{xU1}, is obtained as:

$$\begin{aligned} p_{xU1} &= v_{xU1} i_{xU1} \\ &= \frac{V_{dc} i_{xd}}{4} - \frac{v_x i_x}{4} + \frac{V_{dc} i_x}{8} - \frac{v_x i_{xd}}{2} - v_h i_{xh}. \end{aligned} \tag{25}$$

In (25), it can be seen that the first and second terms are equal each other due to the power balance between the DC input side and AC output side, which is used to derive i_{xd} as:

$$i_{xd} = \frac{v_x i_x}{V_{dc}}. \tag{26}$$

p_{xU1} is derived by substituting (26) into (25), which remains three terms on the right-hand side as:

$$p_{xU1} = \frac{V_{dc} i_x}{8} - \frac{v_x^2 i_x}{2V_{dc}} - v_h i_{xh}. \tag{27}$$

At the low-speed operation, in (27), the first and second terms are low-frequency power fluctuation, whereas the third term, which consists of high-frequency voltage and current (v_h and i_{xh}), generates a constant power and high-frequency power components. The constant power is able to alleviate the low-frequency power fluctuation, which results to high-frequency power component in each half-arm only. As a result, energy in each half-arm and SM capacitor voltage also fluctuates with high frequency, leading to low voltage ripples.

3.3. Control scheme

Fig. 3 shows the control block diagram of the proposed hybrid cross-connected MMC, which is comprised of the leg balancing control, arm balancing control, half-arm balancing control, individual SM balancing control and

individual SM balancing control for series-connection branch. In Fig. 3(a), the leg balancing control is used to force the average SM capacitor voltage in each leg, $\bar{v}_{Cx}$, to follow the SM voltage reference v_C^*. $\bar{v}_{Cx}$ is expressed as:

$$\bar{v}_{Cx} = \frac{1}{2.5N}\left[\sum_{j=1}^{2N} v_{Cj,x} + \sum_{q=1}^{0.5N} v_{CqS,x}\right] \quad (28)$$

where, j is the SM in each arm, q is the SM in each series-connection branch, and $\Delta v_{leg,x}^*$ is the leg voltage command. In addition, i_{xd} is calculated as:

$$i_{xd} = 0.5(i_{xU2} + i_{xL1} + i_{xS}) \quad (29)$$

Since the power difference between the upper and lower arms has been redistributed through the series, the average SM capacitor voltages of the upper and lower arms need to be balanced. Fig. 3(b) shows the control block diagram of the arm balancing control, where $\bar{v}_{C,Ux}$ and $\bar{v}_{C,Lx}$ are the average SM capacitor voltages of the upper and lower arms, respectively. The arm balancing command $\Delta v_{arm,x}^*$ is produced, which includes the high-frequency component. In Fig. 3(a) and (b), the DC and AC-circulating current are inner current loops in the leg and arm balancing controls, which can be considered as circulating current controllers. However, the target is not to eliminate the circulating current as suggested in the grid application.

Fig. 3(c) demonstrates the half-arm balancing control, which is implemented to balance the average SM capacitor voltages between the top and bottom half-arms ($\bar{v}_{C,g1x}$ and $\bar{v}_{C,g2x}$) in the upper and lower arms of each leg. $\bar{v}_{C,g1x}$ and $\bar{v}_{C,g2x}$ is given as:

$$\bar{v}_{C,g1x} = \frac{1}{0.5N}\sum_{j=1}^{0.5N} v_{Cj,xg}\,, \quad (30)$$

$$\bar{v}_{C,g2x} = \frac{1}{0.5N}\sum_{j=0.5N+1}^{N} v_{Cj,xg}\,, \quad (31)$$

where, g = U or L is the upper or lower arms. $\Delta v_{g,x}^*$ is the output voltage command of this controller.

Fig. 3(d) illustrates the control block diagram of the individual SM voltage balancing control, where $v_{Cj,x}$, $i_{xg,k}$ and $\Delta v_{Cj,x}^*$ are the SM capacitor voltage, half-arm current and output voltage command.

Fig. 3(e) shows the control block diagram of the individual SM voltage balancing control in the series-connection branch, where $v_{CjS,x}$ is the SM capacitor voltage and i_{xS} is the branch current.

In addition to the balancing control, the motor control, which is the rotor flux oriented control (FOC) in Fig. 3(f), is also included to produce the output voltage reference, v_x^*, according to the input commands, rotor flux reference and motor speed reference (λ^* and ω_{rm}^*) [23].

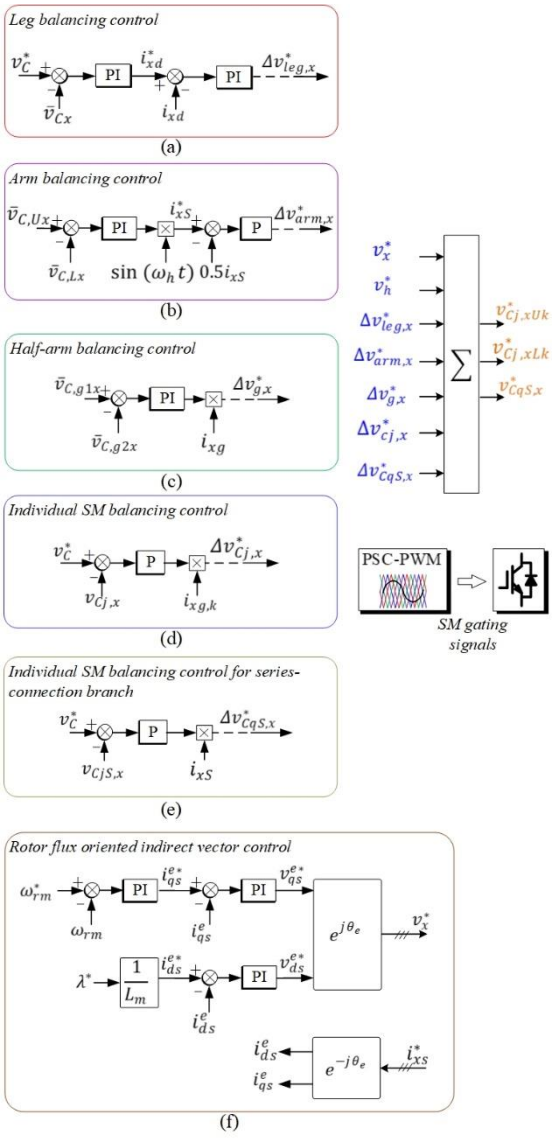

Fig. 3. Control block diagram of hybrid cross-connected MMC. (a) Leg balancing control. (b Arm balancing control. (c) Half-arm balancing control. (d) Individual SM balancing control. (e) Individual SM balancing control for series-connection branch. (f) Rotor flux oriented indirect vector control.

Finally, from the voltage commands of controllers, the voltage references for SMs in the upper arm, $v_{CjU,x}^*$, lower arm, $v_{CjL,x}^*$, and series-connection branch, $v_{CqS,x}^*$, are given as:

$$v_{CjU,x}^* = \frac{V_{dc}}{2N} - \frac{v_x^*}{N}\,\mathrm{m}\,\frac{2v_h^*}{N} - \Delta v_{leg,x}^*\,\mathrm{m}\,\Delta v_{arm,x}^*\,\mathrm{m}\,\Delta v_{U,x}^* + \Delta v_{Cj,x}^*, \quad (32)$$

$$v_{CjL,x}^* = \frac{V_{dc}}{2N} + \frac{v_x^*}{N}\,\mathrm{m}\,\frac{2v_h^*}{N} - \Delta v_{leg,x}^* \pm \Delta v_{arm,x}^*\,\mathrm{m}\,\Delta v_{L,x}^* + \Delta v_{Cj,x}^*, \quad (33)$$

$$v_{CqS,x}^* = \frac{V_{dc}}{2N} - \Delta v_{arm,x}^* + \Delta v_{CqS,x}^* \quad (34)$$

After that, those voltage reference are sent to PWM generator to produce PWM gating signals, which are used to switch IGBT appropriately. The phase-shifted carrier (PSC) modulation with a feature of circulating current harmonics cancellation has been implemented [24]. It means that the displacement angle between the carriers of upper and lower arm is zero.

4. RESULTS AND DISCUSSION

To validate performance of the proposed topology, a 4160-V/1-MW HC-MMC system has been modeled for simulation. The system consists of 30 SMs which are employed in arms and series-connection branches. In Table 1 and 2, the parameters of the HC-MMC and induction motor for the simulation are listed.

Table 1. Converter parameters and ratings

Parameters	Symbol	Value
Apparent power	S	1081 (kVA)
DC link voltage	V_{dc}	7000 (V)
Number of SMs per arm	N	4
Half-arm inductance	L	1.5 (mH)
SM DC voltage	v_C^*	1750 (V)
SM capacitance	C	3000 (μF)
Flying capacitance	C_F	1175 (μF)
Carrier frequency	f_c	2000 (Hz)
Injected resonant frequency	f_r	120 (Hz)

Table 2. Motor parameters and ratings

Parameters	Symbol	Value
Output power	P_o	1250 hp
Rated voltage	V_{LL}	4160 V
Rated current	I_{rated}	150 A
Rated frequency	f_o	60 Hz
Rated speed	ω_{rm_rated}	1189 rpm
Rated torque	T_{rated}	7490 N.m

Fig. 4 demonstrates performance of the HC-MMC at low-speed operation (ω_{rm} = 120 rpm) when the full-load torque is applied. It is significant to control the SM capacitor voltage follow the reference, v_C^*, in order to maintain the desired motor speed and load. Fig. 4(a) shows the three-phase output current with 150A of RMS value. The motor speed is illustrated in Fig. 4(b), where it follows well the reference at 120 rpm under full load condition. In Fig. 4(c), the SM capacitor voltages of phase-*a* are balanced well at 1750 V with 165 V of voltage ripple (9.4% of 1750 -V base). It can be seen that the SM capacitor voltages mainly consists of high-frequency component (120 Hz), which means that the power difference between the upper and lower arms and redistributed well through the series-connection branch. It is similar for SM capacitors in phase-*b* and phase-*c*. Fig. 4(d) and Fig. 4(e) shows the SM capacitor and flying-capacitor voltages in the series-connection branch, where the SM capacitor voltages balanced at the reference well with 260 V of fluctuation. The CMV is shown in Fig. 4(f) with an RMS value of 610 V, which confirms that the injection of high-frequency voltage in each half-arm have no effect on the CMV in the motor side.

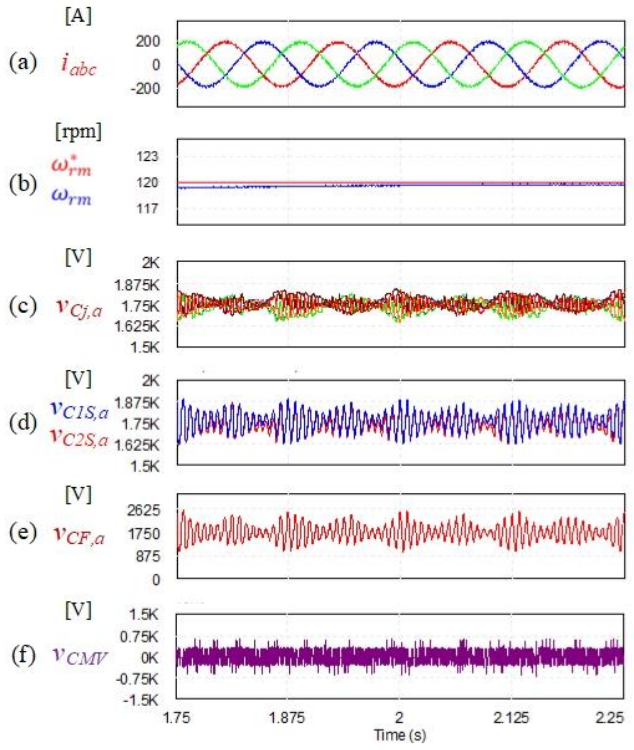

Fig. 4. System performance at the low-speed operation (ω_{rm} = 120 rpm) under full-load condition. (a) Three-phase output current. (b) Motor speed. (c) SM capacitor voltages in phase-*a*. (d) SM capacitor voltages in series-connection branch. (e) Flying-capacitor voltage. (f) Common-mode voltage.

Fig. 5 illustrates performance of the HC-MMC with a start-up operation; then, the load is applied from no load to full load at t = 1.5s, and full load back to no load at t = 2.5s. Fig. 5(a) shows the motor speed, which follow the reference well from the zero speed to 120 rpm. Fig. 5(b) and Fig. 5(c) show the three-phase output current and motor torque. It can be seen that the motor torque change appropriately according to the speed acceleration and load change from no load to full load or from full load back to no load. Due to load changes, there are undershoot and overshoot in the motor speed. The SM capacitor voltages in phase-*a* are demonstrated in Fig. 5(d), which are balanced at the reference (1750 V). It means that the power difference between the upper and lower arms of the proposed topology

are redistributed well in order to alleviate the SM capacitor voltage ripples. Therefore, the voltage ripples are mitigated once the full load is applied. Fig. 5(e) and Fig. 5(f) show the SM capacitor and flying-capacitor voltages in the series-connection branch. The CMV is shown in Fig. 5(g) which has not increased during the load change condition.

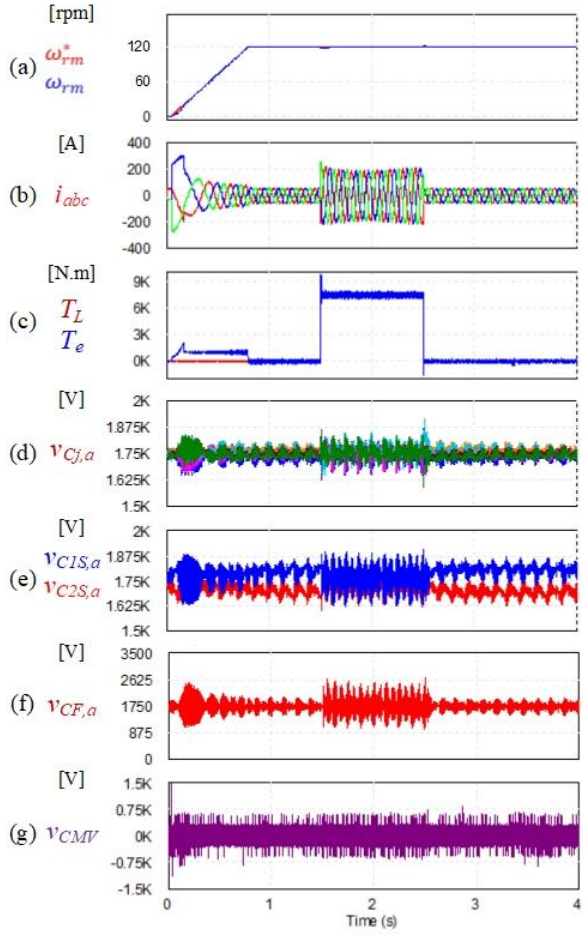

Fig. 5. System performance with the accelerating process from zero speed to 120 rpm and the load change condition. (a) Motor speed. (b) Three-phase output current. (c) Load torque. (d) SM capacitor voltages in phase-*a*. (e) SM capacitor voltages in series-connection branch. (f) Flying-capacitor voltage. (g) Common-mode voltage.

Fig. 6 shows the accelerating performance of the system from zero to rated speed (1189 rpm). The motor speed is illustrated in Fig. 6(a), where it follows the reference well with any distortion. Fig. 6(b) and Fig. 6(c) show the three-phase output current and phase output voltage. During accelerating, the current is higher than that at steady state to generate more torque. It is note that the output voltage level is increased when the motor speed enters the medium or high-speed regions. At the rated speed, nine levels of output voltage are generated. Fig. 6(d) shows the SM capacitor voltage in phase-*a*, which is balanced at the reference well with allowable voltage ripples. In addition, the SM capacitor voltage ripples are only needed to mitigate at the low-speed region since those ripples are naturally shrunk at the high-speed region (0.3 p.u. – 1 p.u.). Therefore, it is not necessary to inject the high-frequency CMV and circulating current at the high-speed region which results in power losses reduction. The SM capacitor and flying-capacitor voltages in the series-connection are shown in Fig. 6(e) and Fig. 6(f). The CMV is demonstrated in Fig. 6(g) with a low peak-to-peak value. At t = 2.05s, since the induction motor operates at the rated speed, the amplitude of three-phase output current is decreased.

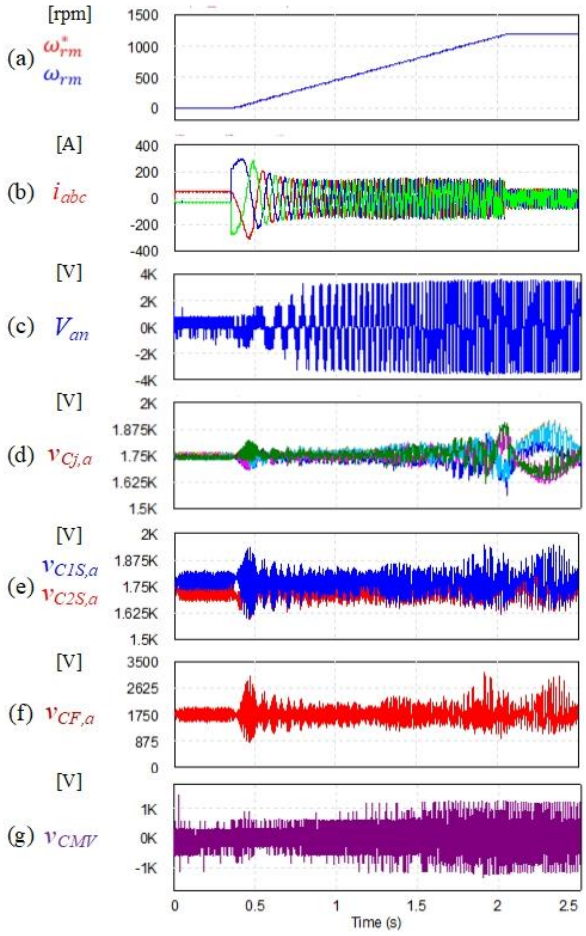

Fig. 6. Accelerating performance of the system from zero to rated speed. (a) Motor speed. (b) Three-phase output current. (c) Phase output voltage. (d) SM capacitor voltages in phase-*a*. (e) SM capacitor voltages in series-connection branch. (f) Flying-capacitor voltage. (g) Common-mode voltage.

5. CONCLUSIONS

In this paper, a hybrid cross-connected modular multilevel converter (HC-MMC) for medium-voltage motor drive applications has been proposed, where the power difference between the upper and lower arms is redistributed through the suggested series-connection branches of the flying-capacitor and HBSMs. Therefore, it is able to operate the motor at low-speed operation with low AC voltage ripple on submodule capacitor without the injection of the common-mode voltage in the motor side. By proposing the series-

connection branch, the rating voltage of flying-capacitor using in the branch is lower than that in the conventional topology. The validity of the proposed HC-MMC and control scheme have been verified through simulation results.

ACKNOWLEDGEMENTS

This work was funded by Ho Chi Minh City University of Food Industry—Contract Number 144/HD-DCT dated 31 December 2019.

REFERENCES

[1] Lesnicar, A. and Marquardt, R. 2003. An innovative modular multilevel converter topology suitable for a wide power range. Proceeding in IEEE Bologna PowerTech Conference, 1–6.

[2] Allebrod, S.; Hamerski, R.; and Marquardt, R. 2008. New transformerless, scalable modular multilevel converters for HVDC-transmission. Proceeding in IEEE Power Electronics. Specialists Conference 174–179.

[3] Le, D. D. and Lee, D.-C. 2022. A modular multilevel converter topology with novel middle submodules to reduce capacitor voltage fluctuations. IEEE Transactions on Power Electronics 37 (1): 70–75.

[4] Nguyen, V.- T; Kim, J.W.; Park J.-W; Lee, J.-M.; and Park, B.- G. 2022. A modified submodule of modular multilevel converter using active power decoupling method for reducing capacitor voltage ripple under low- frequency operation. IET Power Electronics (00): 1–15.

[5] Hagiwara, M. and Akagi, H. 2009. Control and experiment of pulsewidth-modulated modular multilevel converters. IEEE Transactions on Power Electronics 24 (7): 1737–1746.

[6] Solas, E.; Abad, G.; Barrena, J. A.; Aurtenetxea, S.; Carcar, A.; and Zajac, L. 2013. Modular multilevel converter with different submodule concepts-part II: experimental validation and comparison for HVDC application. IEEE Transactions on Industrial Electronics 60 (10): 4536–4545.

[7] Peralta, J.; Saad, H.; Dennetière, S.; Mahseredjian, J.; and Nguefeu, S. 2012. Detailed and averaged models for a 401-level MMC-HVDC system. IEEE Transactions on Power Delivery 27 (3): 1501–1508.

[8] Peng, F. Z.; Lai, J.-S.; McKeever, W.; and Coevering, J. V. 1996. A multilevel voltage-source inverter with separate dc sources for static VAr generation. IEEE Transactions on Industry Application 32 (5): 1130–1138.

[9] Hagiwara, M.; Nishimura, K.; and Akagi, H. 2010. A medium-voltage motor drive with a modular multilevel PWM inverter. IEEE Transactions on Power Electronics 25 (7): 1786–1799.

[10] Korn, A. J. ; Winkelnkemper, M.; and Steimer, P. 2010. Low output frequency operation of the modular multi-level converter. Proceeding in IEEE Energy Conversion Congress Exposition: 3993–3997.

[11] Le, D. D.; Hong, S.; and Lee, D.-C. 2022. Fault detection and tolerant control for flying-capacitor modular multilevel converters feeding induction motor drives. *Journal of Power Electronics 22* (6): 947–958.

[12] Debnath, S.; Qin, J.; and Saeedifard, M. 2015. Control and stability analysis of modular multilevel converter under low-frequency operation. IEEE Transactions on Industrial Electronics 62 (9): 5329–5339.

[13] Hagiwara, M.; Hasegawa, I.; and Akagi, H. 2013. Start-up and low-speed operation of an electric motor driven by a modular multilevel cascade inverter. IEEE Transactions on Industry Applications 49 (4): 1556–1565.

[14] Antonopoulos, A.; Ängquist, L.; Norrga, S.; Ilves, K.; Harnefors, L.; and Nee, H. P. 2014. Modular multilevel converter AC motor drives with constant torque from zero to nominal speed. IEEE Transactions on Industry Applications 50 (3): 1982–1993.

[15] Antonopoulos, A.; Ängquist, L.; Harnefors, L.; and Nee, H. P. 2015. Optimal selection of the average capacitor voltage for variable-speed drives with modular multilevel converters. IEEE Transactions on Power Electronics 30 (1): 227–234.

[16] Zhao, F.; Xiao, G.; Zhu, T.; Zheng, X.; Wu, Z.; and Zhao, T. 2020. A coordinated strategy of low-speed and start-up operation for medium-voltage variable-speed drives with a modular multilevel converter. IEEE Transactions on Power Electronics 35 (1): 709–724.

[17] Le, D. D. and Lee, D.-C. 2022. Current stress reduction and voltage total harmonic distortion improvement of flying-capacitor modular multilevel converters for AC machine drive applications. IEEE Transactions on Industrial Electronics 69 (1): 90–100.

[18] B. Li *et al.* 2016. An improved circulating current injection method for modular multilevel converters in variable-speed drives. IEEE Transactions on Industrial Electronics 63 (11): 7215–7225.

[19] Le, D. D. and Lee, D.-C. 2020. Reduction of half-arm current stresses and flying-capacitor voltage ripples of flying-capacitor MMCs. IEEE Access 8: 180076–180086.

[20] Du, S.; Wu, B.; Zargari, N. R. and Cheng, Z. 2017. A flying-capacitor modular multilevel converter for medium-voltage motor drive. IEEE Transactions on Power Electronics 32 (3): 2081–2089.

[21] Le, D. D.; Lee, D.-C.; and Kim, H.-G. 2020. Three-phase flying-capacitor MMC with six coupled inductors. Journal of Power Electronics 20 (4): 916–925.

[22] Du, S.; Wu, B.; Tian, K.; Zargari, N. R.; and Cheng, Z. 2016. An active cross-connected modular multilevel converter (AC-MMC) for a medium-voltage motor drive. IEEE Transactions on Industrial Electronics 63 (8): 4707–4717.

[23] Krueasuk W.; Bhasaputra P.; and Pattaraprakorn W. 2011. Feasible Study of Restructuring Used Induction Motor for Low Speed Renewable Resource Generator GMSARN International Journal 05 179-188

[24] Wangsathitwong, S.; Sirisumrannukul, S.; Chatratana S.; and Deleroi, W. 2008. Control of Single Phase PWM Converter for Renewable Energy System Using Active and Reactive Current Components GMSARN International Journal 02 67-74.